

Estimation of the neuromodulation parameters from the planned volume of tissue activated in deep brain stimulation

Estimación de los parámetros de neuromodulación a partir del volumen de tejido activo planeado en estimulación cerebral profunda

Viviana Gómez-Orozco^{1*}, Mauricio Alexander Álvarez-López¹, Óscar Alberto Henao-Gallo¹, Genaro Daza-Santacoloma², Álvaro Ángel Orozco-Gutiérrez¹

¹Grupo de Automática, Facultad de Ingenierías, Universidad Tecnológica de Pereira. Carrera 27 # 10-02 Barrio Álamos. A. A. 97. Pereira, Colombia.

²Instituto de Epilepsia y Parkinson del Eje Cafetero - Neurocentro. Carrera 9 # 25-20 Torre A Consultorio 418. C. P. 660002. Pereira, Colombia.

ARTICLE INFO

Received May 29, 2015
Accepted October 27, 2015

KEYWORDS

Deep brain stimulation, planned volume of tissue activated, neuromodulation parameters, support vector machines

Estimulación cerebral profunda, volumen de tejido activo planeado, parámetros de neuromodulación, máquina de soporte vectorial

ABSTRACT: Deep brain stimulation (DBS) is a therapy with promissory results for the treatment of movement disorders. It delivers electric stimulation via an electrode to a specific target brain region. The spatial extent of neural response to this stimulation is known as volume of tissue activated (VTA). Changes in stimulation parameters that control VTA, such as amplitude, pulse width and electrode configuration can affect the effectiveness of the DBS therapy. In this study, we develop a novel methodology for estimating suitable DBS neuromodulation parameters, from planned VTA, that attempts to maximize the therapeutic effects, and to minimize the adverse effects of DBS. For estimating the continuous outputs (amplitude and pulse width), we use multi-output support vector regression, taking the geometry of the VTA as input space. For estimating the electrode polarity configuration, we perform several classification problems, also using support vector machines from the same input space. Our methodology attains promising results for both the regression setting, and for predicting electrode active contacts and their polarity. Combining biological neural modeling techniques together with machine learning, we introduce a novel area of research where parameters of neuromodulation in DBS can be tuned by manually specifying a desired geometric volume.

RESUMEN: La estimulación cerebral profunda (ECP) es una terapia con resultados promisorios para el tratamiento de desórdenes del movimiento. Esta envía estimulación eléctrica por medio de un electrodo a una región específica del cerebro. La propagación espacial de la respuesta neuronal a esta estimulación se conoce como volumen de tejido activado (VTA). Cambios en los parámetros de estimulación que controlan el VTA, como la amplitud, el ancho de pulso y la configuración de polaridad del electrodo pueden afectar la efectividad de la terapia ECP. En este estudio, desarrollamos una metodología novedosa para estimar los parámetros de neuromodulación de ECP adecuados, a partir del VTA planeado, que trata de maximizar los efectos terapéuticos y minimizar los efectos adversos de la ECP. Para la estimación de las salidas continuas (amplitud y ancho de pulso), usamos regresión de soporte vectorial de múltiples salidas, tomando la geometría del VTA como espacio de entrada. Para la estimación de la configuración del electrodo desarrollamos varios problemas de clasificación, también utilizando máquinas de soporte vectorial para el mismo espacio de entrada. Nuestra metodología logra resultados prometedores tanto en el caso de regresión como para predecir los contactos activos del electrodo y su polaridad. Combinando técnicas de modelamiento de neuronas biológicas junto con aprendizaje de máquina, se introduce una novedosa área de investigación donde los parámetros de neuromodulación en ECP pueden sintonizarse manualmente especificando un volumen geométrico.

* Corresponding author: Viviana Gómez Orozco
e-mail: vigomez@utp.edu.co
ISSN 0120-6230
e-ISSN 2422-2844

1. Introduction

Deep brain stimulation (DBS) is a therapy used for the treatment of neurological conditions, such as Parkinson's Disease, essential tremor, and dystonia, among others. It is considered when drug therapy cannot suitably control the movement disorder symptoms. DBS involves the placing of an electrode within a target brain region (the basal ganglia, the thalamus, or other subcortical structures). Although DBS is an effective therapy, understanding the effects of neuronal response to electrical stimulation (its action mechanisms) remains unclear [1-3]. The fundamental purpose of DBS is to modulate neural activity with applied electric fields [4]. In this regard, a measure of the effects of deep brain stimulation is to estimate the volume of tissue activated (VTA), namely, the spatial spread of direct neural response to external electrical stimulation via a deep brain stimulation (DBS) electrode [5, 6].

Once the DBS electrode is implanted, one essential step is the configuration of the neurostimulation parameters. The neurostimulation is carried out by different active contacts in the electrode. Each active contact generates a rectangular pulse function, that shares the same amplitude, pulse width, and frequency. Furthermore, a contact could be active or inactive. If a contact is active, it can behave as a cathode or anode. Therefore, the neurostimulation parameters are the amplitude, pulse width, and frequency of the rectangular pulse function, and each lead contact configuration (cathode, anode or no stimulation). Although the frequency is an important parameter in DBS, it is considered that it does not have an influence in VTA estimation [7]. Accordingly, in this paper, we consider as neurostimulation parameters the amplitude, and pulse width of the rectangular pulse function, and the configuration of each lead contact.

Variations in the electric stimulation parameters affect the spread of the activation, which can have serious consequences on therapeutic effects, or induce side effects when such parameters are not carefully adjusted [8]. The process for manually getting the right parameters can be quite time-consuming since it usually relies on the experience of the medical specialist, commonly demanding several clinical sessions for a successful result. Therefore, in order to achieve the desired therapeutic benefits, and to reduce the amount of time spent by the patient and the specialist in clinical sessions, it is important to find a procedure for optimally adjusting the DBS device parameters.

Although there is a huge amount of literature on the subject of computing the VTA given a specific set of neuromodulation parameters [5-7, 9], the inverse problem, this is, the problem of computing a set of specific neuromodulation parameters given a desired VTA, has received less attention. A previous study about the estimation of VTA uses an approach based on artificial neural networks to characterize the stimulation parameters adjustment effects over DBS [10, 11]. A system is provided in [11], which seeks the correlation between the calculated, and the desired VTA, that allows them to determine the appropriate stimulation parameters for the desired volume. The drawbacks of this approach are that it can not appropriately represent high stimulation parameter values and/or complex electrode configurations (more than

two active contacts), and the assumption of an isotropic tissue medium.

In this work, we propose a novel methodology which allows us to find a suitable configuration of the neurostimulation parameters that attempts to maximize the therapeutic benefits, and to minimize the side effects of the VTA for DBS treatment. We first employ a computer simulator of the VTA generation process, where the input data corresponds to different configurations of the neuromodulation parameters, and the output data corresponds to the graphical representation of the VTA. The simulator uses a model to compute the extracellular potential generated by the DBS, plus a model for estimating the neural activation that takes place due to the electrical stimulation. We refer to this step as the direct problem (it is also known as the forward problem). We then solve an inverse problem that takes as input space the graphical representation of the VTA, and the output space corresponds to the values of the parameters that we want to adjust. To solve the inverse problem, we employ a framework based on support vector machines using them either for multi-output regression (for simultaneously tuning the amplitude and the pulse width), or for classification (for tuning the configuration of each contact). The relevance of the SVM underlies in its robustness for generalization, and its ability for easily dealing with high-dimensional input spaces.

To the best of our knowledge, this is the first attempt to compute the neurostimulation parameters for DBS starting from the desired VTA by the specialist. Results are promising and show that the combination of carefully specified physiological models together with machine learning techniques can be used to tackle a novel problem in DBS.

2. Materials and methods

2.1. Direct problem

The key neurostimulation parameters in VTA estimation are amplitude, pulse width and electrode contacts configuration. In this work, we use a clinical DBS electrode (Medtronic DBS 3389 electrode, ACTIVA-RC stimulator [12]) which offers wide neurostimulation parameter ranges. In clinical studies, the DBS amplitude should not exceed a certain value that depends on the neurostimulator, e.g 3.6 V for the Soletra, and 5.5 V for the Kinetra neurostimulator. To observe changes in patient response, 0.5 V steps in amplitude levels are also needed [13].

The solution of the direct problem in VTA uses two models, the first one to compute the extracellular potential generated by the DBS electrode, and the second one to estimate the neural activation in response to the electrical stimulation [14]. The model that computes the extracellular potential was implemented in COMSOL Multiphysics 4.2. (Comsol Inc., Stockholm Sweden) [15], and it is used to solve Poisson's equation by means of the finite element method (FEM). The model that estimates the amount of neural activation was computed using Neuron 7.3, configured as a Python module [16, 17]. Figure 1 is

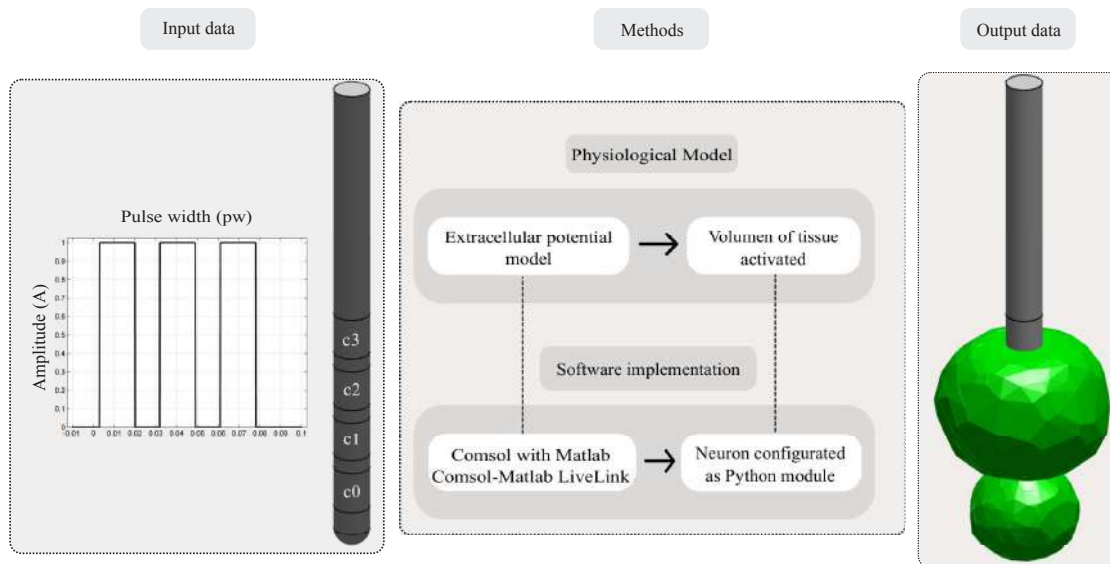


Figure 1 Graphical representation of the methodology used for solving the direct problem. First, the neurostimulation parameters (amplitude, pulse width, and conductive contacts configuration) are selected. Then, an extracellular potential model is executed, in the finite element method (FEM) software COMSOL Multiphysics 4.2., to compute the spatial and temporal distribution of the extracellular potential generated by the neurostimulation parameters. After that, a model of multicompartment myelinated axons is implemented, in NEURON 7.3 configured as a Python module, to determine axonal response to the electric stimulation. Finally, the volume of tissue activated is computed as the volume generated by the active axons

a schematic representation of the methodology used to obtain the solution of the direct problem.

In what follows, we briefly explain the extracellular potential model, and the computation of the volume of tissue activated.

Extracellular potential model

A simplified 3D model of a clinical DBS electrode positioned in the middle of a conductive extracellular medium with an isotropic conductivity [18] was built in COMSOL Multiphysics 4.2., and save as model M-file. The electrode model consisted of four conductive contacts (with a conductivity of $\sigma = 4 \times 10^6 \text{ Sm}^{-1}$) 1.27 mm in diameter and 1.5 mm in height separated by insulating bands ($\sigma = 1 \times 10^{-10} \text{ Sm}^{-1}$) 0.5 mm in height, and of an insulating semicircular tip with radius 0.635 mm (Figure 2). The conductor extracellular medium consisted of a sphere of diameter 10 cm. It was assumed to be homogeneous and isotropic with conductivity $\sigma = 0.3 \text{ Sm}^{-1}$, relative permittivity $\epsilon_r = 80$ [18], and an encapsulation tissue layer of 0.5 mm around the electrode with conductivity of $[V_0 = 0 \text{ V}]$ [7, 19]. The DBS pulse was modeled as a rectangular pulse by imposing time dependent Dirichlet boundary conditions on the contacts of the DBS electrode considered as actives. The remaining contacts were left inactive. Dirichlet boundary conditions $[V_0 = 0 \text{ V}]$ were also imposed on the boundaries of the extracellular medium. Finally, zero current flow conditions were imposed

on the surfaces of the non active contacts, and insulating components of the electrode [7]. The Poisson's equation was used to compute the spatial and temporal distribution of the extracellular potential.

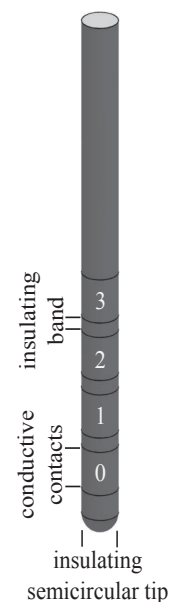


Figure 2 A simplified 3D model of the DBS 3389 electrode. Four conductive contacts (numbered from 0 to 3 and separated by insulating bands), and an insulating semicircular tip comprise the simplified model

Once the extracellular potential model was built, it was run into Matlab 2012a using COMSOL with Matlab (COMSOL-Matlab LiveLink) [20]. We automated the solution of the Poisson's equation for several possible neurostimulation parameter combinations (Table 1) by using an M-file in Matlab. A random sample of 500 neurostimulation configurations was taken for the available parameter values under study (Table 1), where each configuration described amplitude, pulse width, and the active contacts during the electrode stimulation.

Table 1 Set of possible neurostimulation parameters and electrode configuration used in this work

Parameter	Range
Amplitude (A)	0.5-5.5 V in 0.5 V steps
Width pulse (W)	60-450 μ s in 30 μ s steps
Contact 0 (c_0) ^a	0; -1; 1
Contact 1 (c_1)	0; -1; 1
Contact 2 (c_2)	0; -1; 1
Contact 3 (c_3)	0; -1; 1

^aNo stimulation (0), cathodal stimulation (-1), anodal stimulation (1)

Volume of tissue activated

The gold standard for VTA estimation consists in coupling the electric potential due to DBS with a model of multicompartment myelinated axons distributed around the electrode shaft. The volume of tissue activated is computed as the volume generated by the active axons. To compute the change in the transmembrane potential induced by the stimulation, the multicompartment myelinated axonal model [14, 21] was implemented in Python 2.7 with Neuron 7.3 configured as a Python module. Each axon includes 21 nodes of Ranvier, and 2 myelin attachment segments (MYSA), 2 paranode main segments (FLUT), and 3 internode

segments (STIN) between each node. For more detailed information, see [22]. The axonal field was modeled as fibers of 5.7 μ m diameter. The straight axons were oriented in four different directions, perpendicular to the axis of the electrode, and positioned at a distance between axons of 0.5 mm in both the vertical and horizontal directions [21]. The electrical potential was interpolated from the elements of the FEM mesh onto each of the sections that integrated the axonal model.

Computer emulator of the simulation model

Solving exactly the model for the multicompartment myelinated axons described above is computationally expensive. For each neurostimulation parameter configuration, running the full simulation model takes around one hour. In order to reduce the computational complexity of computing 500 times the direct problem, we used a computer emulator for the simulation model. The computer emulator was based on a Gaussian process (GP) classifier. The GP classifier was trained to emulate the action of the gold standard for VTA estimation, that is, it was trained to determine the spatial extent of neuronal activation, predicting which axons were activated by the applied extracellular stimulus [23]. The GP emulator reduces the computation time to about four mins [23], allowing the complete computation of 500 samples in a reasonable time. The methodology used for emulating the multicompartment myelinated axonal model is summarized in Figure 3. Our final dataset is made of 500 values for the neurostimulation parameters together with the 500 geometrical VTAs generated by each configuration.

It is important to clarify that each VTA was estimated for the same elements of the FEM mesh with labels {0; 1} that determine which of these elements were not activated (label 0) or were activated (label 1) (see Figure 4). The applied stimulus was different for each sample.

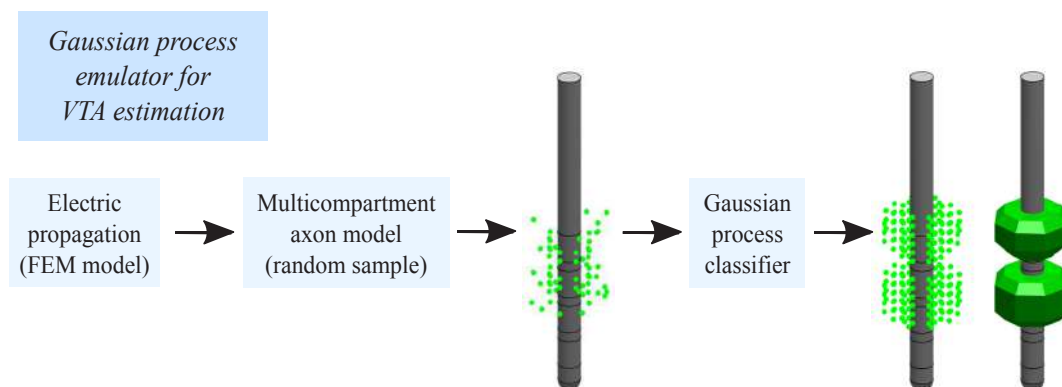


Figure 3 Graphical representation of the methodology used to emulate the VTA generated by the multicompartment myelinated axonal model. First, the electric potential generated by the DBS electrode is computed by means of the finite element method (FEM). Then, the multicompartment axon model is executed by a random sample from the total axonal population, in order to simulate of the axonal response to the electric stimulation. This information is used to train a Gaussian process classifier to emulate the action of the gold standard for VTA estimation

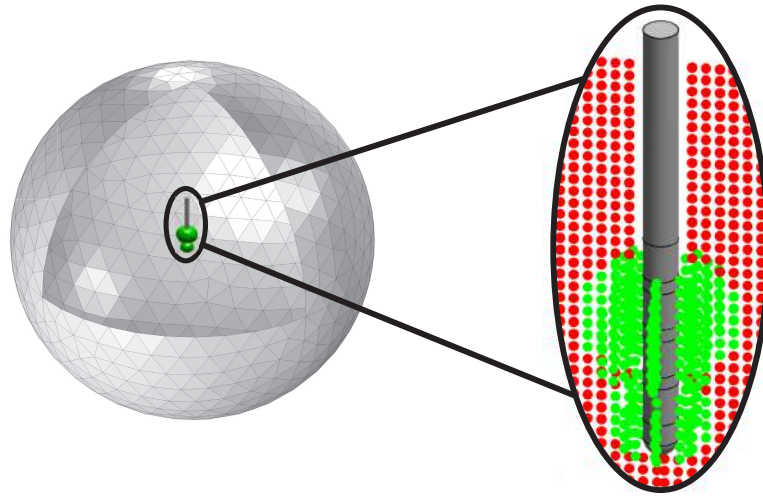


Figure 4 The sphere represents the region of interest (subthalamic nucleus), where the direct problem was solved. Elements of the FEM mesh are closer together around the electrode than in other places. This is to improve the precision of the solution around the electrode. Green dots are elements labeled active ('1'), and red dots are elements labeled not active ('0'). We want to clarify that green and red dots are not superposed, it is a 3D image snapshot

2.2. Inverse problem

Each geometrical representation of the VTA is described using an m -dimensional vector made of zeros, and ones. A value of zero in this vector indicates that the mesh element of the finite element solution (from the direct problem) was inactive due to the particular configuration of the neurostimulation parameters. A value of one in this vector indicates that the mesh element was active. The value of m is determined by the elements of the FEM mesh (in our case, $m = 177,924$), that is, the elements necessary to cover a spherical volume of 10 cm centered around the subthalamic nucleus, our target brain region for DBS.

As explained in the introduction, we want to map the geometrical representation of the VTA to the neurostimulation parameters that were used for computing that VTA. In short, we want to build a vector-valued function f that maps m -dimensional binary vectors \mathbf{x} , to a six-dimensional vector $\mathbf{y} = [A \ W \ c_0 \ c_1 \ c_2 \ c_3]^T$, where A refers to the amplitude of the pulse, W refers to the pulse width, and c_k refers to the condition of contact k , with $k = 0; 1; 2; 3$.

The space of the brain region that we want to cover with the VTA leads to vectors \mathbf{x} with a dimensionality m greater than a thousand, depending of the volume resolution that we aim for the VTA. For building functions in such high dimensional input spaces, we use a framework based on Support Vector Machines, where the computations involved are dependent on the number of samples (in our case, less than 500 for the training stage), and not on the dimensionality of the input space.

For constructing the function $\mathbf{y} = f(\mathbf{x})$, we use two types of support vector learners. We jointly model the amplitude $A(\mathbf{x})$, and the pulse width $W(\mathbf{x})$ using multiple-

output support vector regression through the scheme proposed in [24, 25]. Although, we could use support vector regression for modeling $A(\mathbf{x})$, and $W(\mathbf{x})$ independently, we experimentally found that modeling them jointly offered better results. This result is expected since in generating the VTA, both $A(\mathbf{x})$, and $W(\mathbf{x})$ are correlated. We also modeled the contacts c_0, c_1, c_2 , and c_3 as four different classification tasks, using support vector classifiers for each of them. The methodology employed for solving the inverse problem is depicted in Figure 5.

The subject of multiple-output regression in the context of SVMs has been less studied in the literature, and in what follows, we briefly summarize the theory behind [24, 25]. The theory behind support vector classifiers is well-known, and it can be found in different machine learning textbooks [26, 27].

For all the SVM configurations (multiple output regression, and the independent classification tasks), we use a kernel function $k = (\mathbf{x}, \mathbf{x}')$ based on a Hamming distance $D_H = (\mathbf{x}, \mathbf{x}')$ between the binary vectors \mathbf{x} , and \mathbf{x}' , vectors obtained from the mesh given by the FEM model. The Hamming distance measures the number of positions at which the corresponding vectors, \mathbf{x} and \mathbf{x}' , have different symbols. For the SVMs, we also tried the classical radial basis function (RBF) kernel, but the results were extremely poor. The RBF kernel might be useful when the input space is continuous, which is not our case.

Support vector regression for multiple outputs

The SVM regression method for multiple outputs that we use in this work is an approach, which defines a hyper-sphere insensitivity zone, that allows us to penalize only once the

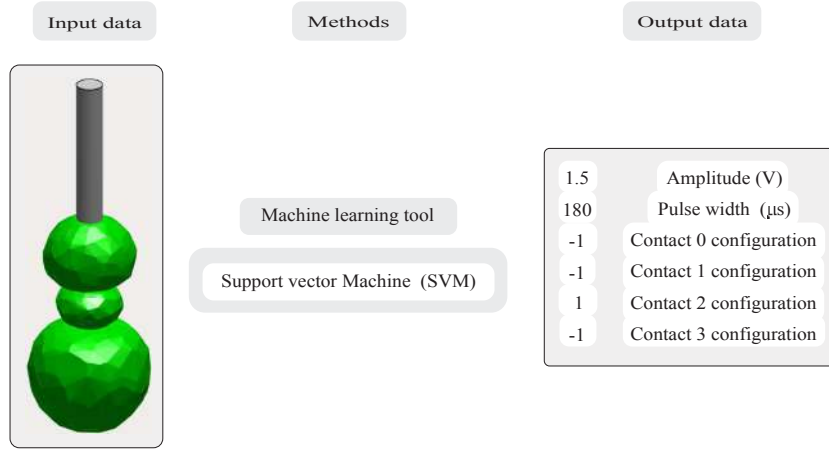


Figure 5 Graphical representation of the methodology used to solve the inverse problem. First, the direct problem is executed several times for different configuration parameters. Then, a dataset is built for the neurostimulation parameters together with the geometrical VTAs. This information is used to train a support vector machine to obtain the neurostimulation parameters of a specific geometry of the VTA

samples that are not placed inside the insensitivity zone for solving multiple outputs regression problems [24, 25, 28]. Let $\mathbf{x}_i \in \mathbb{R}^m$ be the input vector, and $\mathbf{y} \in \mathbb{R}^Q$ the output vector. The relationship between \mathbf{x} , and \mathbf{y} is assumed to follow, Eq. (1)

$$\mathbf{y} = \mathbf{W}^T \phi(\mathbf{x}) + \mathbf{b}, \quad (1)$$

where $\mathbf{W} = [\mathbf{w}^1, \dots, \mathbf{w}^Q]$, $\mathbf{b} = [b^1, \dots, b^Q]^T$ a regressor \mathbf{w}^j and b^j for every output. The function $\phi(\mathbf{x})$ refers to a non-linear transformation to a higher-dimensional space d , where $d \gg m$.

Given a dataset $\{\mathbf{x}_i, \mathbf{y}_i\}_{i=1}^n$, the purpose is to find the set of parameters $\{\mathbf{W}, \mathbf{b}\}$ that minimize the objective function (Eq. (2))

$$L_p(\mathbf{W}, \mathbf{b}) = \frac{1}{2} \sum_{j=1}^Q \|\mathbf{w}^j\|^2 + C \sum_{i=1}^n L(u_i), \quad (2)$$

where C is a regularization constant, $L(u_i)$ is a loss-function, with $u_i = \sqrt{\mathbf{e}_i^T \mathbf{e}_i}$ and $\mathbf{e}_i = \mathbf{y}_i - \mathbf{W}^T \phi(\mathbf{x}_i) - \mathbf{b}$. As a loss function $L(u_i)$, the authors of [25] use a quadratic loss (Eq. (3)) with respect to an user defined constant ϵ

$$L(u) = \begin{cases} 0, & u < \epsilon \\ (u - \epsilon)^2, & u \geq \epsilon. \end{cases} \quad (3)$$

An iteratively reweighted least squares (IRLS) procedure is used to estimate the parameters \mathbf{W} , and \mathbf{b} .

The solution of the problem above can also be expressed in terms of the vector of coefficients β^j for each output, which relates to the original vectors \mathbf{w}^j through $\mathbf{w}^j = \Phi^T \beta^j$, where $\Phi = [\phi(\mathbf{x}_1), \dots, \phi(\mathbf{x}_n)]^T \in \mathbb{R}^{n \times d}$. The prediction \mathbf{y}^* for a new input vector \mathbf{x}^* can be

computed as $\mathbf{y}^* = \mathbf{K}_* \beta + \mathbf{b}$, where $\beta = [\beta^1, \dots, \beta^Q]$, and \mathbf{K}_* is the kernel between \mathbf{x}^* and the training set.

Procedure with SVMs

For all the experiments with SVMs (multi-output regression, and classification), we performed training with seventy percent observations in the dataset, this is, 350 sample points; and testing, with thirty percent of the data, this is, 150 sample points. In the four classification problems (c_0 , c_1 , c_2 , and c_3) we employed the PRTools Matlab toolbox [29], with our own kernel function. For each of these classification problems, the classes considered were three, namely, active contact behaving as anode (label 1), active contact behaving as cathode (label -1), and inactive contact (label 0). The performance measure that we report for classification is the accuracy. For the multi-output regression problem, we use the code provided in [30]. The performance measure that we report for regression is the relative difference between the test value and the predicted value (the relative difference between two values x , and y is defined as $|x - y| / \max(x, y)$, where $|x|$ is the absolute value of x , and $\max(x, y)$ is the maximum value between x , and y). In both cases, the experiments were run 20 times with different training and testing sets to assess the performance.

We also evaluate the performance of the different SVM in terms of the dimensionality m of the input vectors \mathbf{x} , in other words, in terms of the spatial resolution of the VTA. We start with a dimensionality of $m = 177,924$, and then we uniformly subsample each vector by factors of 10; 50, and 100, obtaining input spaces of dimensionalities $m = 17,793$, $m = 3,559$ and $m = 1,780$, respectively. Figure 6 shows an example of the geometries of the VTA for the different input data resolutions considered.

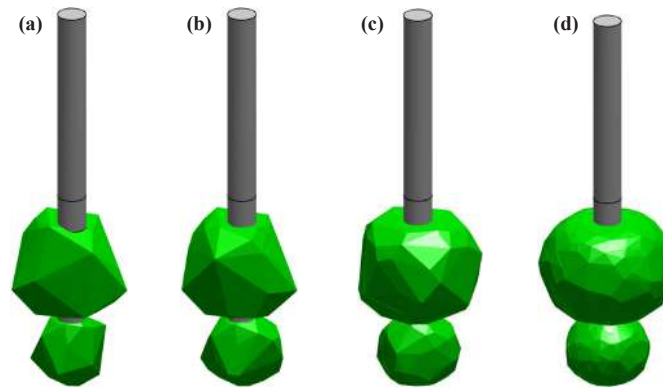


Figure 6 Graphic representation of the VTA geometry taking different resolution values to asses behavior of SVM under lower dimensional input data ($A = 1.0 V, W = 390 \mu s, c_0 = 1, c_1 = -1, c_2 = -1, c_3 = 0$), where (a) $m = 1,780$. (b) $m = 3,559$. (c) $m = 17,793$. (d) $m = 177,924$.

We use different statistical tests to study if there are differences that are significant among the performances obtained in terms of the dimensionality m , for a particular classification task, or for the multiple-output regression task. First, we apply a Lilliefors test for normality over the 20 repetitions of each value of m . If the null hypothesis for normality is rejected, we perform a Kruskal-Wallis test to compare median performances among the values of m , otherwise we use ANOVA. If the null hypothesis for equal medians is rejected, we perform a multiple comparison test using Tukey-Kramer to study further which performances in terms of m are different. All the significance levels are measured at 5%. Details for this procedure can be found in [31].

3. Results

3.1. Direct problem

The main objective of the direct problem is to model a DBS electrode inside the brain tissue, onto a region of interest, under ideal assumptions, to modulate the neural activity. The idea is to deliver an electrical pulse to the target region, and then to study the neural response to this stimulation that is well-known as VTA. Figure 7 shows the potential distribution for a specific neurostimulation parameter setting and the corresponding estimated VTA.

3.2. Generated dataset

The purpose of the dataset generated was to capture different parameter configurations and their corresponding VTAs. Figure 8 shows six samples of possible parameter combinations (see Table 1), and how they affect the volume that represents the spatial spread of neural activation due to the electric stimulation. A monopolar stimulation, with a low amplitude and a high pulse width value, is represented in Figure 8(a), it shows that high values of pulse width induce a small neural response. A bipolar stimulation, anode-cathode, is described by Figure 8(b), while a cathode-cathode is described by Figure 8(e). The relevance in this

configuration is to show how the polarity affects the VTA. The other Figures (Figure 8(c), Figure 8(d) and Figure 8(f)) allow us to see the influence of the parameter variations onto the estimated volume.

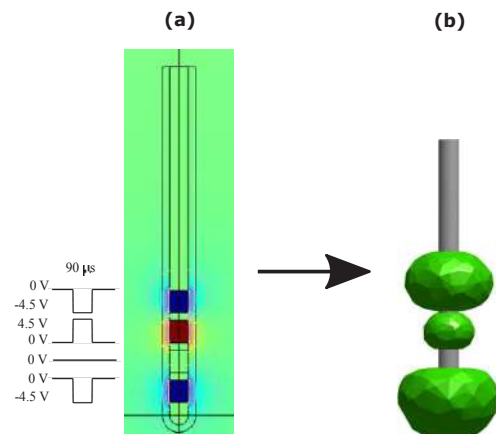


Figure 7 Graphic representation of the model that solves the direct problem. (a) Extracellular potential generated by the DBS electrode in Comsol Multiphysics ($A = 4.5 V, W = 90 \mu s, c_0 = -1, c_1 = 0, c_2 = 1, c_3 = -1$), with a schematic representation of the stimulation delivered through each electrode contact. (b) Estimated VTA induced by the electrical stimulation

3.3. Inverse problem

Table 2 summarizes the accuracy obtained for each classification task in terms of the different resolutions of the input data. We obtain a slightly better accuracy for contacts c_0, c_1 and c_3 when the dimensionality of the input data is $m = 17,793$. The best result for contact c_2 was obtained when the dimensionality of the input space was equal to $m = 177,924$. We apply the statistical significance test described in section II-B2 for each classification task, obtaining as a result that the performances for all the contacts are not statistically different in terms of the value

of m . This result can be explained by the fact that we are assuming isotropic conductivities for the extracellular potential model, and the shapes for the different VTA generated have regular forms. We expect that if we work with anisotropic conductivities, the shapes generated for the VTA will have irregular forms, and the dimensionality of the input space will become a relevant parameter. Based on the results of Table 2, we conclude that the classification accuracy is in the range of 81% (an error rate of 19%) for contact c_2 , and 88% (an error rate of 12%) for contact c_1 .

differences are not significant for the amplitude, nor for the pulse width. Again, this could be explained due to the regular forms of the VTA as a consequence of the isotropic conductivities used in the extracellular potential model. The relative difference for the amplitude is about 24%, whereas the relative difference for the pulse width is about 30%.

Table 3 Relative differences for the amplitude and pulse width with several values of the dimensionality x for the input space x

Dimensionality m of x	Amplitude [V]	Pulse width [μ s]
1,780	0.2478±0.1913	0.3027±0.1878
3,559	0.2449±0.1910	0.2963±0.1887
17,793	0.2453±0.1901	0.2973±0.1894
177,924	0.2462±0.1901	0.2980±0.1892

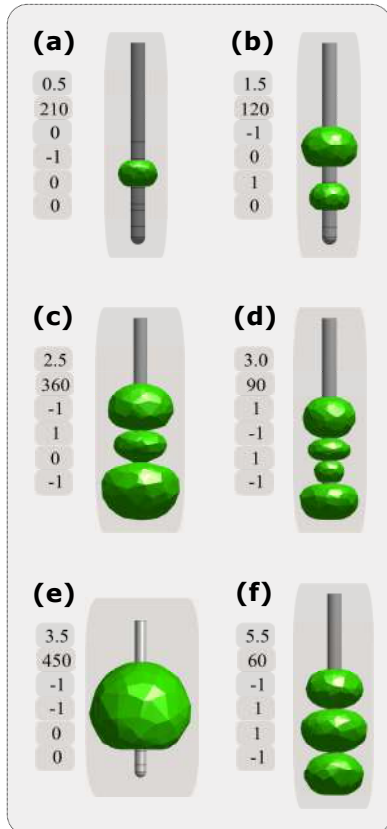


Figure 8 Graphic representation of different samples of the dataset generated, and their respective amplitude (V), pulse width (μ s) values, and electrode configuration

Table 3 shows the relative difference for the amplitude and the pulse width, in terms of the dimensionality m of the input space. Applying the statistical tests described before, we find that the discrepancies among the relative

4. Discussion and conclusions

In this study, we developed a novel methodology to address the problem of finding optimal neurostimulation parameters that increase the effectiveness of the DBS therapy. Our method, first builds a dataset of volumes of tissue activated with their corresponding neurostimulation parameters. This dataset is built with an accurate physiological model that combines an extracellular potential model, and a multicompartiment myelinated axonal model. We then use this dataset to design a machine learning algorithm that maps from the space of volumes of tissue activated to the values of the neurostimulation parameters. Since the representation of each VTA is given as a long vector of zeros and ones, in this paper, we use a kernel machine, a SVM, that allows us to handle spaces of high dimensionality. We obtain classification accuracies over 80% for predicting the states of the electrode contacts, and relative differences equal or lower than 30% for the amplitude and the pulse width of the rectangular pulse function. To the best of our knowledge, this is the first attempt in the literature for DBS, that looks to automatically tune the neurostimulation parameters from a previously specified VTA. Although the results shown in this paper may be considered as preliminary, we think these results are promising, and leave plenty of room for further improvement. First, in this paper we solved

Table 2 Accuracy in each electrode contact configuration (anodal, cathodal or no stimulation) with different values of dimensionality m of the input space x

Dimensionality m of x	Contact 0 [c_0]	Contact 1 [c_1]	Contact 2 [c_2]	Contact 3 [c_3]
1,780	0.8757±0.0224	0.8269±0.0420	0.7953±0.0231	0.8660±0.0283
3,559	0.8754±0.0204	0.8343±0.0407	0.8088±0.0247	0.8656±0.0317
17,793	0.8813±0.0217	0.8460±0.0416	0.8166±0.0265	0.8693±0.0285
177,924	0.8795±0.0216	0.8457±0.0407	0.8174±0.0257	0.8663±0.0292

the classification problems and the regression problems independently. We hope that by solving simultaneously the classification and regression problems, we may improve the performance metrics. This is a foundational idea in successful frameworks like transfer learning or multi-task learning. Second, the choice of the kernel may also help to improve the results. We would like to experimentally test the performance under different distance or similarity measures (other than the Hamming distance), and under different and more sophisticated kernels that exploit the geometric structure of the VTA [32, 33]. Third, the experiments of this paper show that it is possible to reduce the dimensionality of the input space without affecting the performance metrics. Reducing the dimensionality of the input space may ease the design of the machine learning model, improving the performance for classification and regression.

On a different line of work, we would like to apply the methodology for more realistic scenarios, for example, by using anisotropic conductivities for the extracellular potential model, reflecting the properties of the different brain tissues. Such anisotropic conductivities can be obtained from magnetic resonance imaging. For this type of study, it will be important to analyze the performance of the method for different patients.

5. Acknowledgment

The authors would like to thank “Universidad Tecnológica de Pereira” for providing us with the computational resources needed to perform the direct problem. This research is developed under the project “Estimación de los parámetros de neuro modulación con terapia de estimulación cerebral profunda en pacientes con enfermedad de parkinson a partir del volumen de tejido activo planeado”, financed by Colciencias with code 111065740687. The author VGO was also supported by the 645 agreement, “Jóvenes Investigadores e Innovadores”, funded by Colciencias. The author GDS was partially supported by Colciencias project 499153530997. We would like to thank Iván De La Pava for helping with the direct problem. We would also like to thank the authors of [25] for providing the code of multiple-output regression.

6. References

1. C. McIntyre, W. Grill, D. Sherman and N. Thakor, “Cellular effects of deep brain stimulation: model-based analysis of activation and inhibition”, *Journal of Neurophysiology*, vol. 91, no. 4, pp. 1457-1469, 2004.
2. C. McIntyre and P. Hahn, “Network perspectives on the mechanisms of deep brain stimulation”, *Neurobiology of Disease*, vol. 38, no. 3, pp. 329-337, 2010.
3. R. So, A. Kent and W. Grill, “Relative contributions of local cell and passing fiber activation and silencing to changes in thalamic fidelity during deep brain stimulation and lesioning: a computational modeling study”, *Journal of Computational Neuroscience*, vol. 32, no. 3, pp. 499-519, 2012.
4. A. Chaturvedi, C. Butson, S. Lempka, S. Cooper and C. McIntyre, “Patient-specific models of deep brain stimulation: influence of field model complexity on neural activation predictions”, *Brain Stimulation*, vol. 3, no. 2, pp. 65-77, 2010.
5. C. Butson and C. McIntyre, “Tissue and electrode capacitance reduce neural activation volumes during deep brain stimulation”, *Clinical Neurophysiology*, vol. 116, no. 10, pp. 2490-2500, 2005.
6. C. Butson, S. Cooper, J. Henderson and C. McIntyre, “Patient-specific analysis of the volume of tissue activated during deep brain stimulation”, *Neuroimage*, vol. 34, no. 2, pp. 661-670, 2007.
7. N. Yousif *et al.*, “Evaluating the impact of the deep brain stimulation induced electric field on subthalamic neurons: a computational modelling study”, *Journal of Neuroscience Methods*, vol. 188, no. 1, pp. 105-112, 2010.
8. J. Volkmann, J. Herzog, F. Kopper and G. Deuschl, “Introduction to the programming of deep brain stimulators”, *Movement Disorders*, vol. 17, pp. 181-187, 2002.
9. N. Yousif, R. Borisyuk, N. Pavese, D. Nandi and P. Bain, “Spatiotemporal visualization of deep brain stimulation-induced effects in the subthalamic nucleus”, *European Journal of Neuroscience*, vol. 36, no. 2, pp. 2252-2259, 2012.
10. A. Chaturvedi, J. Luján and C. McIntyre, “Artificial neural network based characterization of the volume of tissue activated during deep brain stimulation”, *Journal of Neural Engineering*, vol. 10, no. 5, 2013.
11. J. Luján, A. Chaturvedi and C. McIntyre, “System and method to estimate region of tissue activation”, U.S. Patent 8589316. Nov. 19, 2013.
12. Medtronic, *DBS Lead Kit for Deep Brain Stimulation*, 2002. [Online]. Available: <http://www.medtronic.com/downloadablefiles/UC199901079bEN.pdf>. Accessed on: Dec. 16, 2014.
13. American Association of Neuroscience Nurses (AANN), *Care of the Movement Disorder Patient with Deep Brain Stimulation*, AANN Clinical Practice Guideline Series, 2009. [Online]. Available: <http://www.aann.org/pdf/cpg/aanndeepbrainstimulation.pdf>. Accessed on: Dec. 16, 2014.
14. F. Rattay, “Analysis of models for extracellular fiber stimulation”, *IEEE Transactions on Biomedical Engineering*, vol. 36, no. 7, pp. 676-682, 1989.
15. COMSOL Multiphysics, *COMSOL Multiphysics User's Guide (Version 4.2)*. Stockholm, Sweden: COMSOL, 2011.
16. M. Hines and N. Carnevale, “The NEURON simulation environment”, *Neural Computation*, vol. 9, no. 6, pp. 1179-1209, 1997.
17. M. Hines, A. Davison and E. Muller, “NEURON and Python”, *Frontiers in Neuroinformatics*, vol. 3, pp. 1-12, 2009.
18. T. Zhang and W. Grill, “Modeling deep brain stimulation: point source approximation versus realistic representation of the electrode”, *Journal of Neural Engineering*, vol. 7, no. 6, 2010.

19. C. Butson, C. Maks and C. McIntyre, "Sources and effects of electrode impedance during deep brain stimulation", *Clinical Neurophysiology*, vol. 117, no. 2, pp. 447-454, 2006.
20. D. Kern and N. Framke, *Automation of COMSOL Multiphysics Parameter Studies using the MATLAB Livelink*, 2012. [Online]. Available: https://www-user.tu-chemnitz.de/~dker/tutorial_comsol_matlab_livelink.pdf. Accessed on: Dec. 18, 2014.
21. G. Walckiers, "Bio-electromagnetic model of deep brain stimulation", Ph.D. dissertation, École polytechnique fédérale de Lausanne, Lausanne, Switzerland, 2009.
22. C. McIntyre, A. Richardson and W. Grill, "Modeling the excitability of mammalian nerve fibers: influence of afterpotentials on the recovery cycle", *Journal of Neurophysiology*, vol. 87, no. 2, pp. 995-1006, 2002.
23. I. Pava *et al.*, "A Gaussian Process Emulator for Estimating the Volume of Tissue Activated During Deep Brain Stimulation", in *7th Iberian Conference on Pattern Recognition and Image Analysis (IbPRIA)*, Santiago de Compostela, Spain, 2015, pp. 691-699.
24. F. Pérez *et al.*, "Multi-dimensional function approximation and regression estimation", in *International Conference on Artificial Neural Networks (ICANN)*, Madrid, Spain, 2002, pp. 757-762.
25. M. Sánchez, M. de Prado, J. Arenas and F. Pérez, "SVM multiregression for nonlinear channel estimation in multiple-input multiple-output systems", *IEEE Transactions on Signal Processing*, vol. 52, no. 8, pp. 2298-2307, 2004.
26. B. Scholkopf and A. Smola, *Learning with Kernels: Support Vector Machines, Regularization, Optimization, and Beyond*, 1st ed. Cambridge, USA: MIT Press, 2001.
27. C. Bishop, *Pattern recognition and machine learning*, 1st ed. New York, USA: Springer, 2006.
28. D. Tuia, J. Verrelst, L. Alonso, F. Pérez and G. Camps, "Multioutput support vector regression for remote sensing biophysical parameter estimation", *IEEE Geoscience and Remote Sensing Letters*, vol. 8, no. 4, pp. 804-808, 2011.
29. R. Duin *et al.*, *PRTools4, A Matlab Toolbox for Pattern Recognition*, Delft University of Technology, 2007. [Online]. Available: <http://www.prtools.org/files/PRTools4.1.pdf>. Accessed on: Jan. 15, 2015.
30. F. Pérez, *MSVR: Multioutput Support Vector Regression*. [Online]. Available: <http://www.uv.es/gcamps/software.html>. Accessed on: Jan. 15, 2015.
31. J. Pizarro, E. Guerrero and P. Galindo, "Multiple comparison procedures applied to model selection", *Neurocomputing*, vol. 48, no. 1, pp. 155-173, 2002.
32. F. Bach, "Graph kernels between point clouds", in *25th international conference on Machine Learning*, Helsinki, Finland, 2008, pp. 25-32.
33. S. Vishwanathan, N. Schraudolph, R. Kondor and K. Borgwardt, "Graph kernels", *The Journal of Machine Learning Research*, vol. 11, pp. 1201-1242, 2010.